Role of Surfactants and Salt in Aqueous Two-Phase Separation of Carbon Nanotubes toward Simple Chirality Isolation

Navaneetha K. Subbaiyan,[†] Sofie Cambré,[†,‡] A. Nicholas G. Parra-Vasquez,[†] Erik H. Hároz,[†] Stephen K. Doorn,[†] and Juan G. Duque[†,*]

[†]Chemistry Division, Physical Chemistry and Applied Spectroscopy Group (C-PCS) and Center for Integrated Nanotechnologies (CINT), Los Alamos National Laboratory, Los Alamos, New Mexico 87544, United States, and [‡]Experimental Condensed Matter Physics Laboratory, University of Antwerp, Belgium

ABSTRACT Aqueous two-phase extraction has recently been demonstrated as a new method to separate single-wall carbon nanotubes (SWCNTs). In this work, we determined that the mechanism of separation is driven by the hydrophobicity of the surfactant, or combination of surfactants, at the SWCNT surface. This knowledge allowed us to develop a simple approach for obtaining highly enriched single-chirality suspensions in only 1 or 2 steps. These results were obtained by strategically combining multiple surfactants with different diameter-dependent binding affinities for SWCNTs and salts that readjust the surfactant structure within the mixed micelle surrounding the SWCNTs. The procedure is successfully applied to SWCNTs from different sources (CoMoCAT and HiPco) with various diameter distributions (from 0.53 to 1.2 nm). Each separation step is characterized by optical absorption, resonant Raman, and photoluminescence excitation spectroscopies. By determining the SWCNT sorting mechanism, we were able to develop a new set of parameters that separated another chirality.

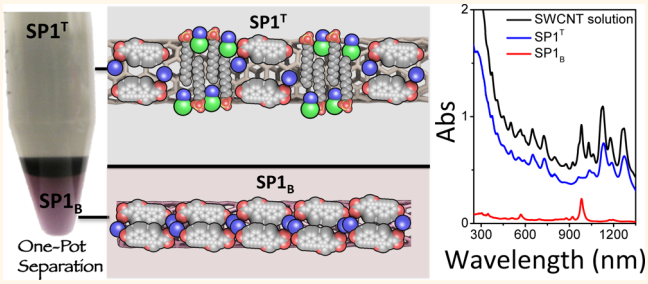

KEYWORDS: carbon nanotubes · sorting · chirality · surfactant structure · phase separation · ATPE · one-pot separation

The unique and remarkably diverse electronic and optical properties of single-wall carbon nanotubes (SWCNTs) have proven to be extremely interesting for various applications.[1] Synthesis methods, however, generally produce inhomogeneous mixtures in chirality, diameter, band gap, *etc.* This is a critical problem for some applications that demand nanomaterials with more uniform properties. Since electronic and optical properties depend critically on the SWCNT structure, there is a significant interest in postsynthesis methods to separate SWCNTs to obtain single- or few-chirality dispersions. Numerous separation methods that provide nearly single-chiralities have been reported, such as selective dispersibility using short DNA segments followed by ion exchange chromatography,[2] selective dispersibility by designed polymers,[3] and suspending the SWCNTs with surfactants in aqueous dispersions followed by gel chromatography[4] or density gradient ultracentrifugation (DGU).[5] These techniques, however, have their drawbacks, such as high cost and low accessibility (*e.g.*, DNA-based ion exchange chromatography, selective dispersibility), numerous iterations to achieve high purity (gel chromatography, DGU) and long separation times, thereby preventing low-cost scale-up of the method.

Recently, a new method has been introduced showing promise of an easily accessible and highly scalable route for generating a wide range of enriched chirality materials.[6] The aqueous two-phase (ATP) separation method[7] is based on the spontaneous redistribution of carbon nanotubes into two aqueous phases with relatively different hydrophobicity. The two phases are formed by mixing two water-soluble polymers, such as polyethylene glycol (PEG) and dextran, in appropriate concentrations. The top phase, mainly containing PEG, is less hydrophilic than the bottom,

* Address correspondence to jduque@lanl.gov.

Received for review November 15, 2013 and accepted January 22, 2014.

Published online January 22, 2014
10.1021/nn405934y

dextran-rich phase. Initially it was hypothesized that the SWCNT separation was driven by the intrinsic hydrophobicity of the SWCNT chiralities, independent of surfactant concentrations.[6] However, in recent work,[8] it has been shown that by varying the concentration of sodium deoxycholate (DOC) and sodium dodecylsulfate (SDS), SWCNTs show diameter-dependent separation. In fact, controlled stepwise changes in DOC and SDS concentrations result in highly enriched SWCNT suspensions of specific small diameters no matter the chiral type (metallic/semiconducting),[8] suggesting there is more than just intrinsic SWCNT hydrophobicity driving the ATP separations. Similarly, in DGU separation, systems containing multiple surfactants are known to form mixed micellar structures (SDS:DOC[9] or SDS:SC[10]) that alter the density surrounding the SWCNT allowing a type separation by density. These micelle structures are strongly dependent on the exact ratio between the two surfactants.

ATP separation of SWCNTs is a newly introduced technique with significant room for improvement: fewer steps to achieve a desired chirality should increase yields and simplicity (previously 6−10 steps[8]), determining the overall surfactant concentrations required to obtain one specific chirality will improve reproducibility and reduce the number of steps, and expanding the technique to a wide range of starting materials will enhance method versatility (previously, single-chirality ATP separations have only been demonstrated on CoMoCAT SG65i samples with a rather narrow diameter/chirality distribution[8]). Mechanistic understanding of the process should lead to simple parameter adjustments to "dial-in" a chirality of interest.

In previous work, we have demonstrated that electrolyte addition is capable of adjusting both the surfactant structure and equilibrium concentrations surrounding the SWCNTs. In particular, after NaCl addition, diameter-dependent aggregation due to surrounding surfactant depletion was observed[11] and density-based separations were improved through surfactant density reorganization.[12] Therefore, these salt-dependent phenomena, which have shown diameter-dependent selectivity, should provide a new tuning parameter to improve and better understand the ATP separation method.

In this work, we unravel the ATP mechanism by carefully tuning the specific co-surfactant concentrations and introducing salt as a means to alter the surfactant structure around the SWCNTs. We are able to achieve nearly single-chirality (6,5) dispersions in only two steps from various source materials, dramatically improving the yield of the separation. With only two required steps and precise control of ingredient concentrations, this approach is simple to reproduce and scale up. Furthermore, we systematically studied the effect of each ingredient on the separation process during both steps. Specifically, the addition of NaCl is critical in isolating (6,5) from different sources, even those in which the (6,5) chirality represents a minority fraction. Also, the relative chirality separation is extremely sensitive to DOC and SDS concentrations. In fact, we find that the formation of mixed micelles, which strongly depends on the specific SDS:DOC ratio, and the resulting surface structure of the surfactants in the presence of salt, determines the overall hydrophobicity, which drives the separation. Detailed understanding of the sorting mechanism leads to a rational adjustment of our two-step procedure to separate other chiralities (*e.g.*, the (7,5) SWCNT) as well.

RESULTS AND DISCUSSION

SWCNTs are known to be polydisperse in diameter/chirality when produced, leading to variability in the starting material chirality distributions with respect to production batch and method. Therefore, three SWCNT batches, known to vary in chiral distribution (CoMoCAT SG65i, HiPco 164.4 and HiPco 195.2), are studied in this work (see Figure 1A). CoMoCAT SG65i material (black trace) predominantly consists of (6,5) SWCNTs (absorption at 980 nm for the first optical transition (E_{11}) and 570 nm for the second optical transition (E_{22}), as indicated by the dashed lines in Figure 1A), HiPco 164.4 material (blue trace) only contains a very low percentage of (6,5) SWCNTs and

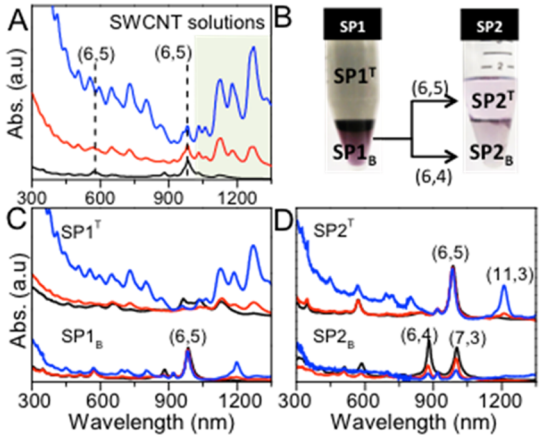

Figure 1. (A) Absorption spectra of the three different SWCNT samples dispersed in 1.04% (m/v) DOC in H_2O. The first and second absorption features of the (6,5) tube are indicated by the dashed lines; (black) CoMoCAT SG65i SWCNTs, (red) HiPco 195.2 batch, and (blue) HiPco 164.4 batch. The main difference between the samples is the ratio of (6,5) tubes to larger diameter tubes in the sample (highlighted by the green box). Spectra are normalized to the (6,5) absorption feature at E_{11} and vertically shifted for clarity. (B) Sample images after SP1 and SP2, for the CoMoCAT SG65i batch. (C) Absorption spectra of the $SP1_B$ and $SP1^T$ for the different SWCNT suspensions. Spectra were normalized to (6,5) absorption feature at E_{11} in the bottom fraction, and $SP1^T$ absorption spectra are vertically shifted for clarity. (D) Absorption spectra of $SP2^T$ and $SP2_B$ fractions for the different SWCNT suspensions. Spectra were normalized to the (6,5) absorption feature at E_{11} in the top fraction, and $SP2^T$ absorption spectra are vertically shifted for clarity.

a significant number of larger diameters (absorption in the range of 1000−1500 nm, indicated by the shaded area in Figure 1A), and HiPco 195.2 material (red trace) contains a large percentage of both (6,5) and larger diameter SWCNTs.

The separation procedure described here consists of two steps (SP1 and SP2); a resulting image at the end of each step is shown in Figure 1B (see Methods section for detailed information and separation procedure). For each step, we prepared a stock solution (STOCK 1 and STOCK 2), composed of SDS, DOC, sodium cholate (SC), NaCl, dextran and PEG. In SP1, an aqueous SWCNT dispersion in 1.04% mass by volume (m/v) DOC was mixed with STOCK 1 and diluted with nanopure H_2O to achieve a final DOC concentration of 0.047% (m/v) (below its critical micelle concentration (CMC) of 0.09−0.27% m/v at room temperature[13]). The resulting suspension was then benchtop-centrifuged for 5 min to induce phase separation (see Methods section). A select subset of small-diameter chiralities preferentially distributes into the bottom fraction ($SP1_B$), as shown by the changes in color of the dispersion in the image and by the absorption spectra, Figure 1B,C. After SP1, all the larger diameters ($d > 0.76$ nm), other than (11,3), have been redistributed into the top phase ($SP1^T$, Figure 1C and Figure 4A). Thus with only one step, a large separation occurs, leaving a small subset of chiralities in the bottom phase ($d \leq 0.76$ nm, optical density (OD) of the E_{11} of (6,5) ~0.3 (2.5) in 3 mm path-length for HiPco 195.2 (CoMoCAT) batch. (Note that after SP1, the OD of (6,5) is difficult to define accurately due to cross-contamination with (7,3) E_{11} absorption.)) In SP2, STOCK-2 is mixed in equal volumes with $SP1_B$ and centrifuged resulting in the chirality distribution in each phase ($SP2_B$ and $SP2^T$) presented in Figure 1D. $SP2_B$ mainly contains (6,4) and (7,3) SWCNTs, while $SP2^T$ mainly consists of (6,5) SWCNTs (OD of the E_{11} of (6,5) ~0.07 (0.3) in 3 mm path-length for HiPco 195.2 (CoMoCAT) batch). Similar results were obtained regardless of nanotube source (CoMoCAT, HiPco), and thus diameter distribution, highlighting the versatility of this process. Unless otherwise stated, from this point forward, all results are discussed using the HiPco 195.2 material.

Spectroscopic Analysis. The chiral composition of each phase produced from the two separation steps was analyzed by combining the absorption spectra (presented in Figure 1) with photoluminescence excitation (PLE) and resonance Raman spectroscopy (RRS). In particular, RRS at various excitation wavelengths allowed the evaluation of the presence of metallic SWCNTs, which is not possible to determine *via* PLE, as well as larger diameter semiconducting species, which have a lower photoluminescence (PL) quantum efficiency.[14] The RRS spectrum of the starting HiPco 195.2 suspension is compared to the spectra of the top and bottom fractions $SP1_B$, $SP1^T$, $SP2_B$ and $SP2^T$

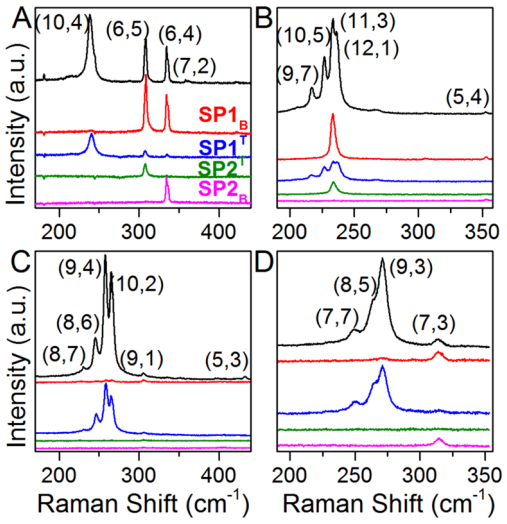

Figure 2. Resonant Raman spectra of the radial breathing modes (RBMs) of the starting HiPco 195.2 suspension (black) and the different fractions after separation, $SP1_B$ (red), $SP1^T$ (blue), $SP2_B$ (magenta), and $SP2^T$ (green). Spectra are vertically shifted for clarity. RRS spectra were obtained at (A) 570 nm, (B) 785 nm, (C) 725 nm, and (D) 514.5 nm. Additional RRS spectra excited at 650, 488, and 457.9 nm can be found in Figure S1.

(Figure 2 and additional spectra in Figure S1). The spectra provide an accurate overview of the chirality redistribution over the different phases (for details see Table S1). The results support a strong diameter-based separation, independent of metallicity, with a clear-cut occurring at 0.747 nm in SP1 and at 0.696 nm in SP2.

Starting from a total of 30 identified chiralities in our spectroscopic window, 9 are isolated in the $SP1_B$ fraction. In SP2, 5 remain in the top phase and 6 in the bottom phase, with some SWCNTs present in both phases. The highly enriched (6,5) sample ($SP2^T$) contains small amounts of (9,1), (11,3), (7,4) and (8,3) SWCNTs. As evaluated from absorption spectra, nearly all the (6,5) SWCNTs separate into this phase or are lost at the interface (see section Separation Yield). The separation technique is so effective that even HiPco 164.4, with minimal (6,5) population, can be significantly enriched in (6,5) (Figure 1), as shown by the reversal of the absorbance ratio of (6,5) to (11,3) (E_{11} wavelength at 1200 nm) between the starting HiPco suspension and $SP2^T$. The highly enriched (6,4)/(7,3) suspension ($SP2_B$) contains also (9,1) and (5,4) and a minimal amount of (8,3) and (12,2) SWCNTs, mostly removed in SP1.

The PLE maps of the different fractions are presented in Figure 3. When these PLE maps were integrated for each chirality over well-defined emission-excitation intervals (Figure S2), the distribution of semiconducting SWCNTs in the different samples was obtained (Figure S3), in full agreement with the RRS observations of diameter-based separation. In particular, the PLE data for $SP2^T$ further indicate the high degree of (6,5) enrichment. We also observed that the

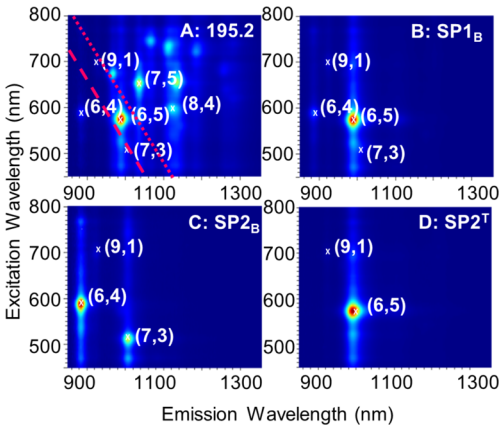

Figure 3. PLE spectra for (A) the starting SWCNT solutions (HiPco 195.2), (B) $SP1_B$, (C) $SP2_B$, and (D) $SP2^T$. Peak positions of the most prominent species are indicated in the figure. The diameter-cut for SP1 (red dotted line) and for SP2 (red dashed line) are also indicated in panel A. Spectra were normalized by maximum signal to better identify SWCNT chiralities present.

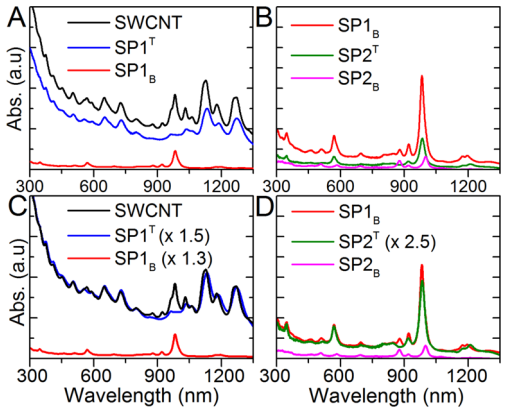

Figure 4. (A and B) Absorption spectra of the starting HiPco 195.2 SWCNT suspension and the different fractions after SP1 and SP2 separation. Absorption spectra are rescaled according to eq 3. (C and D) Absorption spectra additionally rescaled according to the legend, such that the sum of the two spectra after separation matches the starting absorption spectrum. It should be noted that the absorption spectra for the top phase are red-shifted and broadened with respect to the starting SWCNT suspension.

PL quantum efficiency of the (7,3) SWCNTs is much lower than that of the (6,4) SWCNTs, although both have similar optical densities (Figure 1D). This further demonstrates the importance of having nearly single-chirality dispersions to study the optical properties of SWCNTs.

Separation Yield. To obtain a better understanding of the separation yield, the absorption spectra are re-scaled appropriately in Figure 4. We start with a mass balance:

$$M_S = M_T + M_B + M_I \quad (1)$$

where M_j is the mass of the SWCNTs in the starting dispersion (S), top phase (T), bottom phase (B) and the interface (I). The mass can be determined from absorption through an extinction coefficient, ε:

$$M_j = \frac{a_j}{\varepsilon_j} V_j \quad (2)$$

where a_j is absorption and V_j is the volume of the respective phase. Assuming the extinction coefficient does not change significantly in each phase, eq 1 can be rearranged to compare absorbances:

$$a_S = \frac{V_T}{V_S} a_T + \frac{V_B}{V_S} a_B + \Delta Q \quad (3)$$

where ΔQ is the loss of material at the interface. For SP1, $V_S = 215\ \mu L$, $V_B = 900\ \mu L$ and $V_T = 3820\ \mu L$, while for SP2, V_S, V_B, and V_T are all 1 mL. Figure 4A,B presents the absorption spectra of the starting SWCNT suspension (normalized by (6,5) E_{11} resonant absorption) and the rescaled absorption spectra of the $SP1_B$, $SP1^T$, $SP2_B$ and $SP2^T$ fractions according to eq 3. For further comparison, these absorption spectra were multiplied by a certain factor (shown in Figure 4C,D legends) so that the sum of $SP1_B$ and $SP1^T$ would give the initial dispersion absorption spectra; similarly, the sum of $SP2_B$ and $SP2^T$ would give the $SP1_B$ absorption spectra. Thus after SP1, approximately 77% of the (6,5) SWCNTs can be found in the bottom phase and about 67% of the larger diameters in the top phase. All other material is lost at the interface. In SP2, about 60% of the (6,5) SWCNTs are lost at the interface, while the (6,4) and (7,3) SWCNTs maintain their concentration giving overall yields of 31%, 77%, and 77% for the (6,5), (6,4), and (7,3) SWCNTs, respectively. These results show that when the (6,5) SWCNTs pass through the interface to redistribute from the bottom to the top phase in SP2, a significant fraction of the SWCNTs remains at the interface (see also the image in Figure 1B where a dark band is observed at the interface for both separations). Thus, to increase the yield of the separations, it is crucial to limit the number of consecutive steps.

Concentration Effects of Each Component on ATP Separation. To understand the separation mechanism, we isolated the contribution of each component (SDS, SC, NaCl, DOC) in STOCK-1 and STOCK-2 mixtures by varying the concentration (one at a time) and performing the separation procedure. To assess these separations, absorption spectra of $SP1_B$ were obtained (Figure 5, see also Table S2, Figures S4−S10).

SDS Contribution. SP1 separation is very sensitive to SDS concentration (Figure 5A). Without the presence of SDS in STOCK-1 (black curve in Figure 5A), no separation was observed and all SWCNTs remain in the bottom fraction. Upon adding SDS, larger diameter SWCNTs are the first to be removed from the bottom phase and for an optimized amount of SDS (*i.e.*, 1.117 g in 100 mL of STOCK-1) only the smallest diameters ($d \leq 0.76$ nm) remain in the bottom phase. Upon further addition of SDS, (6,5) SWCNTs distribute into the top phase, resulting in a bottom phase that is highly enriched in (6,4)/(7,3) suspension in one step.

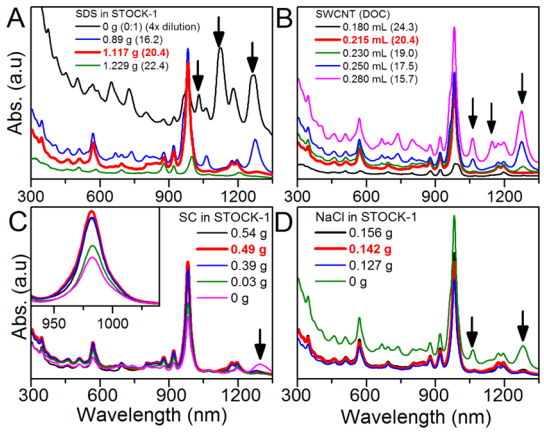

Figure 5. Absorption spectra of $SP1_B$, using the HiPco 195.2 batch. One-by-one variation of (A) SDS, (B) DOC, (C) SC, and (D) NaCl concentration, while keeping all other parameters fixed. SDS:DOC ratios in the final mixture are also provided. The spectrum of the ideal STOCK-1 solution for each graph is presented in red. For SDS, SC, and NaCl, the weight added to 100 mL of the STOCK-1 solution is presented, while for DOC, the final concentration after all components is presented. Arrows highlight the regions in the absorption spectra that are most affected by the variation of the surfactants.

DOC Contribution. SP1 separation is also highly sensitive to DOC concentration (Figure 5B). In the absence of DOC, all SWCNTs separate into the top phase (Figure S4, test 8 and Figure S5), while for a high DOC concentration, all SWCNTs remain in the bottom phase (Figure S4, test 7). As the concentration of DOC decreases, the larger diameter SWCNTs begin to separate to the top phase (not shown), while the smaller diameters remain in the bottom phase (Figures 5B and S6). An ideal DOC concentration for (6,5) isolation in the presence of all other components in STOCK-1 occurs at 0.047% (m/v), corresponding to the addition of 215 μL of the 1.04% (m/v) SWCNT dispersion to the STOCK-1 mixture. Below this concentration, (6,5) SWCNTs reside in the top phase. This suggests that tuning the DOC concentration can control the chiral type separation. In fact, only a 0.003% difference in DOC concentration changes the outcome of the separation (Figures 5B and S6). By stepwise reducing the DOC concentration, it is shown that different chiralities gradually separate into the less hydrophilic top phase, starting with the largest diameters.

SC Contribution. SC has a slightly different chemical structure than DOC (only differs in one hydroxyl group), but has been shown to behave quite differently in metal/semiconducting and chirality separations of SWCNTs by DGU, indicating a very different surfactant wrapping around the SWCNTs.[5,15−17] Although the chemical structures are similar, we find the chiral type separation is less sensitive to the SC concentration (Figure 5C) in comparison to DOC. A final SC concentration above the CMC (in the absence of DOC, see Figure S4, test 9) results in all SWCNTs partitioning into the bottom phase (similar to DOC); however, a final concentration below the CMC results in all the SWCNTs separating into the top phase, while for the same DOC concentration, nearly all SWCNTs remain in the bottom phase (Figure S5B). We find that the effect of adding SC primarily increases the yield of (6,5) SWCNTs in the separation by almost a factor of 2 (see inset Figure 5C) and a faster removal of the larger diameters to the top phase (Figure S7). This suggests that SC preferentially wraps small-diameter SWCNTs, increasing their yield in the bottom phase, while enabling an increase in the SDS coverage of large-diameter SWNTs, thus moving them to the top phase. Noteworthy is the fact that while the yield of the (6,5) SWCNTs is increased by the SC addition, the absorbance of the metallic SWCNTs stays constant, thereby increasing the ratio of (6,5) to (7,4) SWCNTs in this fraction, suggesting a possibility of metallic separation. By analogy, mixed micelles of SDS and SC have shown metal/semiconducting separation with DGU.[5,10]

Salt Contribution. Finally, as observed in Figure 5D, the addition of NaCl helps to separate large diameter SWCNTs into the top phase, and this phenomenon is not very sensitive to the salt concentration. Only at much higher salt concentrations do the (6,5) SWCNTs redistribute into the top phase (Figure S8).

Even though the ATP separation is highly sensitive to the SDS and DOC concentration, we find that the SDS:DOC ratio defines the separation. Specifically, a ratio of 20.4:1 is optimal for (6,5) separation with minimal presence of other chiralities. (Since DOC concentration is much lower than SDS, all SDS:DOC ratios will be greater than 1, so hereafter we will present a ratio of 20.4:1 as just 20.4.) This is confirmed by changing the absolute SDS and DOC concentrations, while maintaining a constant SDS:DOC ratio and achieving the same separation (Figure S9, tests 20−21). Increased absolute throughput is possible by allowing more DOC-dispersed SWCNTs to be added when a greater amount of SDS is used in STOCK-1. However, the absolute concentrations are limited by stability of SWCNTs at higher SDS concentrations (between 3 and 5%).[18] In addition, we performed the same separation using SC- or SDS-dispersed SWCNTs and we prepared the STOCK-1 solutions in such a way that the SDS:DOC ratio in the final separation is the same. We obtained the same separation (Figure S10, tests 22−23) independent of the dispersing surfactant for the initial SWCNTs, verifying that the SDS:DOC ratio determines the separation.

Components in SP2. As with SP1, SP2 is highly sensitive to the specific SDS:DOC ratio (see Figure 6). Reducing the SDS concentration (Figure 6A) or increasing the DOC concentration (Figure 6B) to ratios below 20.8 causes all SWCNTs to collect in the bottom phase. Conversely, lowering the DOC concentration (ratio of 47.2 after mixing) or increasing the SDS concentration

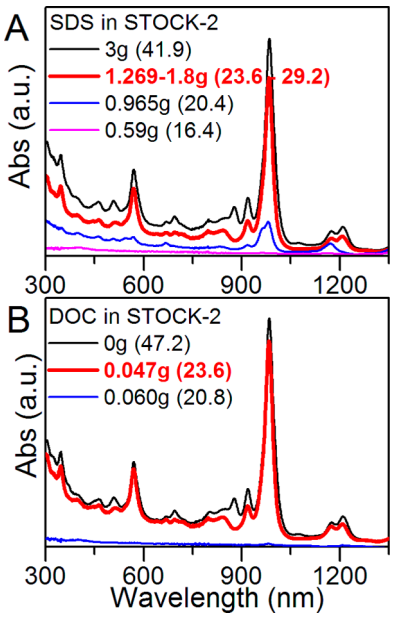

Figure 6. Absorption spectra of SP2^T, while varying the SDS:DOC ratio through addition of (A) SDS or (B) DOC in STOCK-2 (in 100 mL H_2O). The ratios leading to the best separations are presented in red in the legend. The (6,4) (870 nm) and (7,3) (1007 nm) absorption in the top phase increases at higher SDS:DOC ratios indicating more SDS causes smaller diameter SWCNTs to separate into the top phase.

(ratio of 41.9 after mixing) causes all SWCNTs to move to the top phase. Full separation of (6,5) and (6,4)/(7,3) SWCNTs can be achieved by increasing the SDS:DOC ratio in the range of 23.6 to 29.2; in our case, a final DOC concentration of 0.047% (m/v) and SDS concentration in the range of 1.27−1.8% (m/v) in STOCK-2. We find that addition of SC or NaCl to STOCK-2 has no effect on the yield of the separation or removal of large diameter SWCNTs, unlike in SP1, and were therefore omitted from STOCK-2.

Separation Mechanism. *Surfactant and Salt Behavior.* Previous reports show that DOC is a much better surfactant for dispersing SWCNTs than SDS, forming a very homogeneous micelle structure around the SWCNTs, resulting in an increased solubility for individual SWCNTs and an enhanced resolution in optical spectroscopy.[19] DOC tends to stack with its semirigid, hydrophobic, cholesterol-type backbone on the SWCNT walls, while having its flexible polar tail pointed outward to the aqueous environment.[20] In contrast, SDS favors a disordered micellar structure,[21] which in the presence of salts can reorganize into a more densely packed and more highly ordered surface structure.[12,22]

By performing single surfactant ATP separation, we find that DOC-wrapped SWCNTs tend to preferentially reside in the more hydrophilic bottom phase, while SDS-wrapped SWCNTs preferentially reside in the top phase indicating that DOC-SWCNTs are more hydrophilic than SDS-SWCNTs (Figure S5A-B). Even upon addition of salt (up to 60 mM where surfactant reorganization increases the PL QE[12,22]), SDS-covered SWCNTs always separate into the top phase, showing that no matter the structural reorganization, SDS-wrapped SWCNTs are less hydrophilic. At similar salt concentrations, DOC covered SWCNTs remained unaffected (Figure S4), in agreement with previous results.[22] Due to the different hydrophilic nature of pure DOC and SDS micelles, we believe that the exact SDS:DOC ratio and the resulting surfactant structure should influence the ATP separation. Although ATP separation was less sensitive to SC concentration, we performed single surfactant ATP separation of SC-wrapped SWCNTs and found a less definite hydrophobicity effect (Figure S5C). A small amount of all nanotubes remains in both phases, with more small-diameter SWCNTs in the bottom phase and larger diameters in the top phase. This explains our observation that SC increases the yield of small-diameter SWCNTs in the bottom phase and helps separate large-diameter SWCNTs into the top phase.

Indeed, by performing multisurfactant ATP separation, we find that the SDS:DOC ratio determines the specific diameter-cut in the separation. At low SDS:DOC ratios (<20), the larger diameter SWCNTs (>0.76 nm) begin to separate to the top phase, while the smaller diameters remain in the bottom phase (Figures 5B and S6). At higher SDS:DOC ratios (>40), *i.e.*, increasing the SDS concentration, smaller-diameter SWCNTs (<0.76 nm) begin to separate into the top phase. When SC is added, as discussed above, the yield of small-diameter SWCNTs ($d \leq 0.76$ nm) is improved. Due to preferential wrapping of SC, smaller diameters are covered mostly by a mixture of SC and DOC (with minimal SDS), while large-diameter SWCNTs are covered by a mixture of SC, DOC, and SDS.

Finally, the multisurfactant separation is improved by the addition of NaCl, in particular, large-diameter SWCNTs from smaller diameters. Incremental addition of salt results in broadening and slight red-shifts of the optical transitions of the SWCNTs in the top phase (Figure S8). Simultaneously, the higher salt concentrations, as previously reported,[11,12] cause larger diameters to partially aggregate, supported by RRS at 785 nm,[23] resulting in further broadening and greater red-shifts (Figure S8). At high enough salt concentrations, smaller diameter SWCNTs begin to separate into the top phase. As salt concentration increases, the SDS restructuring creates a more favorable environment for SDS on smaller diameter SWCNTs, thus making SDS more competitive with SC to incorporate into the DOC micelle structure, causing these SWCNTs to distribute into the top phase.

Diameter Separation. The mechanism of ATP diameter separation is governed by the surfactants wrapping the SWCNTs, specifically the composition-dependent hydrophobicity of the mixed micelles that are formed. The behavior of the mixed micelle is

defined by a combination of three intrinsic properties of DOC, SC, and SDS: hydrophobicity of the micelles, their relative diameter-dependent SWCNT affinity, and structural reorganization with salt.

We observe that in single surfactant systems each surfactant has different hydrophobicity behavior: DOC is found to be the most hydrophilic surfactant followed by SC and SDS, as evidenced by all DOC-wrapped SWCNTs residing solely in the bottom phase (independent of diameter). In contrast, SDS-wrapped SWCNTs separate into the less hydrophilic top phase, with or without addition of salts. We find that SC also acts as a hydrophilic wrapping, but its behavior is more complex than that of DOC, likely arising from its higher affinity toward the smallest diameters ($d \leq 0.76$ nm). Our results thus also indicate that diameter-dependent differences in binding affinity of the different surfactants will play a role in defining the relative hydrophilicity of the mixed-micelle structures. In agreement with previous reports on surfactant-dependent solubility of tubes,[19,24] we find that SC and DOC have stronger affinities for smaller diameter tubes (with SC the stronger), while SDS has a slightly greater affinity toward larger diameters. This contrasting affinity of SC, DOC, and SDS for different diameter SWCNTs suggests that an increased incorporation of SDS into the large diameter mixed micelles can be possible, resulting in an increased hydrophobicity relative to small diameter SWCNTs.

The addition of salt results in more large-diameter SWCNTs distributing into the top phase (particularly important for separation of the HiPco 164.4 batch containing a significant amount of larger diameters) and at increased concentrations, smaller diameters begin to move toward the top phase or get trapped at the interface. Different factors can play a role in this. First, salt-induced bundling may occur, potentially impacting larger diameters first,[11] causing those to either be trapped at the interface or distribute into the top phase. Additional results on surfactant exchange (see below) indicate, however, that salt-induced bundling likely plays only a minor role for the (6,5) SWCNTs. Second, at lower salt concentrations (those used in these experiments), the structural reorganization of the SDS molecules on the SWCNT surface makes SDS more compatible with the DOC and SC wrapping, even for smaller diameters. The combined diameter-dependent affinity of the surfactants and SDS structural tunability with salts make the mixed micelle formation critically depend on the relative concentrations of SDS, DOC, SC and salt, which define the exact structure formed on the SWCNT surface. The hydrophilicity of the resultant mixed micelle then drives the separation, where greater SDS incorporation, *i.e.*, larger diameters, separate into the less hydrophilic top phase.

Further insight into the mechanism can be obtained by comparing the PL of the (6,5) chirality residing in the bottom ($SP1_B$) and top ($SP2^T$) phases (Figure S11A,B) before and after exchanging the SWCNT/STOCK-1 and -2 dispersion with an aqueous 1% (m/v) DOC solution. In the dextran phase ($SP1_B$), no differences in PL peak position and line width are observed, indicating that little change in surface composition has occurred. This result confirms that after SP1, the (6,5) SWCNTs are mostly covered by DOC molecules (or a mixed micelle of DOC, SC, and possibly insignificant amounts of SDS), and therefore are well-isolated from their environment. For the (6,5) SWCNTs in the PEG phase ($SP2^T$), however, the PL spectrum is clearly red-shifted and broadened compared to the same (6,5) SWCNTs after surfactant-exchange to DOC. Similar red-shift and broadening was obtained upon addition of SDS and salt to a DOC-dialyzed (6,5) SWCNT dispersion (Figure S11C), indicating that the SWCNTs that distribute to the top phase contain SDS within their surfactant layer, after restructuring the SDS in the presence of salts (without the presence of salts, the red-shift is not observed). Such differences in PL with respect to surfactant coverage have also been seen in single surfactant systems.[25,26] Therefore, these results further support the fact that the specific surfactant coverage of the SWCNTs determines their hydrophobicity and that mixed SDS-DOC-SC micelles distribute into the top phase, while mixed micelles with insignificant SDS distribute into the bottom phase.

The SP2 separation follows the same mechanism as described above for SP1. Figure 5A,B shows that at sufficiently high SDS:DOC concentration ratios, above 22.0, the (6,5) SWCNTs tend to redistribute into the top phase. In SP2 the increased SDS:DOC ratio results in more SDS molecules coating the (6,5) SWCNTs, causing them to distribute into the top phase. Similarly, further increasing the ratio moves the even smaller diameter (6,4) and (7,3) SWCNTs to the top phase, confirming that whenever SDS is prevalent in the mixed micelles the SWCNTs reside in the top phase.

In summary, we find the ATP diameter selectivity is governed by the composition of the mixed micelles surrounding the SWCNTs, which in turn is defined by the SDS:DOC concentration ratio. SC and salt are key additives necessary to enhance the separation and yield, and reduce the number of steps in the separation technique; without these, some large-diameter SWCNTs (>0.76 nm) in a diameter-polydisperse sample would remain in both phases. Thus, we were able to separate (6,5) SWCNTs from HiPco batch 164.4, having a larger average-diameter distribution with only a trace amount of (6,5) SWCNTs.

Because the surface species are labile, they can be readily interchanged. The specific mixed micelle compositions and structures that are dependent on SDS:DOC ratio are thus easily adjusted, *even after the phase separation*, to redistribute specific chiralities into another phase. To prove this, we deliberately added less

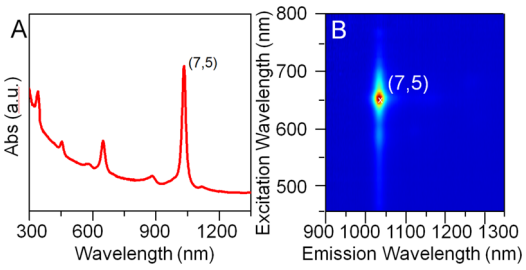

Figure 7. (A) Absorption spectrum of SP2^T after the (7,5) separation from HiPco 195.2 batch and (B) PLE spectrum of the same fraction. Both spectra nicely show the high purity of the (7,5) separation achieved in only two steps.

SWCNT/DOC dispersion (SDS:DOC = 24) in SP1, resulting in (6,5) SWCNTs coated with more SDS molecules and separating into the top phase. We then added more SWCNT/DOC dispersion to make the overall SDS:DOC ratio 20.4 (same as in our standard SP1) and briefly remixed the separated dispersion and centrifuged again. The (6,5) tubes redistributed into the bottom phase, achieving the same separation yield as if it started with 0.047% DOC (Figure S12). This result indicates that, for these smaller diameter SWCNTs, the spectral shifts noted earlier for the top phase solely arise from surfactant reorganization and not bundling. Thus, for obtaining maximum separation yields, the surfactant concentrations can easily be tuned to the desired values. Although the method is highly sensitive to precise surfactant ratios, the relative concentrations can be changed, remixed, and centrifuged to obtain a different separation without decreasing the yield.

Other Chiralities. Overall, changing the SDS:DOC ratio allows very accurate tuning of SWCNT surfactant coverage and thus hydrophobicity, thereby achieving highly enriched chirality dispersions in just 2 steps. By understanding how the different surfactants and salt influence the hydrophobicity, this method can be easily expanded to isolate other chiralities. In Figure S13, we present the variation of the SDS:DOC ratio in SP1 toward (7,5) isolation. An ideal SDS:DOC ratio of 11.7 serves to efficiently transfer (7,5) to the bottom phase after SP1, while limiting other tubes in the bottom phase. In SP2, tuning of the SDS:DOC ratio, similar to the (6,5) separation, allows isolation of both (7,5) and (8,4) (Figure S13, ratio = 11.1) or mainly (7,5) (Figure S13, ratio = 10.4) SWCNTs into the top phase (Figure 7A,B, OD of the E_{11} of (7,5) ~0.06 (0.08) in 3 mm path-length for HiPco 195.2 (CoMoCAT) batch). Thus, by making small changes in surfactant concentration, we successfully separated two chiralities with very small diameter difference (d = 0.83 and 0.84 nm), showing the versatility of our technique and feasibility to apply it to separate any chirality in just two steps.

Scale-Up. ATP metallic/semiconducting separation, a similar technique, was shown to easily scale up on a 1-L scale for arc discharge nanotubes.[6] Here, we easily scaled up our single-chirality method by a factor of 10 (Figure S14), obtaining 4 mL of separated (6,5) SWCNTs after SP1 (OD of E_{11} = 0.25 in 3 mm path-length) in just 15 min. This scale-up was only limited by the size of the centrifugation tubes and benchtop centrifuge available. We also investigated scale-up by increasing the initial SWCNT concentration. Normally 1 mg/mL of raw SWCNTs is used to create a dispersion. We varied the starting concentration from 0.15 to 2.5 mg/mL and found no significant effect on the purity of the (6,5) separation; however, the yield did not scale linearly with starting concentration and no longer increased above 1 mg/mL. Since this technique is not detrimental to SWCNT dispersions, when starting with a (7,5) protocol, the (6,5) SWCNTs in SP2$_B$ can be further separated by adjusting the specific SDS:DOC ratios, as shown previously in reference 8; however, we have accurately determined the specific SDS:DOC ratio necessary to fulfill this separation.

CONCLUSIONS

We have determined that the mechanism for ATP SWCNT separation is driven by the hydrophobicity of the surfactants' composition on the SWCNT surface and not the intrinsic SWCNT hydrophobicity, as previously hypothesized.[6] In particular, when using a mixture of surfactants that have a different diameter-dependent affinity for SWCNTs, we were able to achieve highly enriched single-chirality dispersions of small diameter SWCNTs in just 2 steps, thereby improving chiral sorting of SWCNTs.

We found that DOC micelles create a more hydrophilic surrounding for the SWCNTs compared to SDS, thereby DOC-covered SWCNTs distribute into the more hydrophilic bottom phase while SDS-covered SWCNTs separate into the top phase. Since at low SDS:DOC ratios all SWCNTs are found to be preferentially covered by DOC, no separation occurs. Increasing the SDS:DOC ratio creates competition between both surfactants resulting in mixed micelle coverage and a less hydrophilic surfactant-SWCNT system. Addition of SC results in the formation of mixed SC-DOC micelles for the smaller diameters, and mixed SC-DOC-SDS micelles for the larger diameters, redistributing the latter ones into the less hydrophilic top phase.

Furthermore, addition of salt causes restructuring of the SDS micelles such that SDS is more competitive with SC to cover the SWCNTs, thereby removing the larger diameters and enhancing the chirality separation. We have developed a one-pot procedure to control the surfactant coverage that drives ATP separation and allows isolation of highly enriched (6,5), (6,4)/(7,3) and (7,5) dispersions.

The proposed method is extremely versatile and can be used for various source materials (CoMoCAT or HiPco) to even sort SWCNT chiralities that represent only a minority fraction of the starting material. Moreover, the SDS:DOC ratio can be adjusted at any stage to

separate a desired chirality and the one-pot method is easily scalable. Also, unlike lengthy DGU separations, the short time required for our separation has enabled us to perform many control experiments essential for elucidating a clear separation mechanism. Our findings on the mixed micelle formation will also aid in understanding and improving DGU separations. Furthermore, the understanding of surface interactions presented can be extended to a broader range of chemical systems, including the separation of other nanoscale, low-dimensional systems. Additionally, polarizability differences of small-diameter SWCNTs can, in principle, affect the surfactant structure[12] and composition on their surfaces (as shown also in DGU separations[27]). Thus, by specific surfactant tuning, ATP metal/semiconducting separation of these smaller diameters should be possible, as performed previously on larger diameter arc-discharge nanotubes.[6]

METHODS

CoMoCAT SG65i SWCNTs (SouthWest Nanotechnologies, Lot no. SG65i-L39) and HiPco SWCNTs (Rice University) batch 195.2 and batch 164.4, sodium deoxycholate (DOC, AMRESCO Lot no. 0331C075), sodium cholate (SC, Sigma, Lot no. 040M0156 Aldrich), sodium dodecylsulfate (SDS, Sigma Aldrich, Lot no. SLBD2186V), sodium chloride (Sigma Aldrich C1254), polyethylene-glycol (PEG, MW 6000 Da, Alfa Aesar Lot no.10173268) and dextran (DX, MW 64000−76000 Da, Sigma Aldrich, Lot no. 091M1434V) were used as received

SWCNTs were dispersed in a 1.04% (m/v) DOC solution in nanopure H_2O (ρ = 18.3MΩ·cm) at an initial nanotube concentration of 1 mg/mL, by sonication for 1 h with a tip sonicator (Sonic Vibra Cell with tip CV18-9909, 8W) while immersed in an ice bath. Afterward, the tip-sonicated suspension was centrifuged using an ultracentrifuge (Thermo-Scientific WX-80 Ultra Series with TH-641 rotor) for 2 h at 39191 max *g* and 20 °C. The supernatants (*i.e.*, top 80%) containing the isolated SWCNTs were used for chiral separation.

For SP1, STOCK-1 solution is prepared containing: (i) 14.1 g of PEG, (ii) 4.9 g of dextran, (iii) 0.49 g of SC, (iv) 1.117 g of SDS, (v) 0.142 g of NaCl, and (vi) 100 g of nanopure H_2O. It was mixed overnight using a platform shaker at 150 rpm (New Brunswick Scientific, model C2) to allow all the components to dissolve properly. A total of 215 μL of the 1.04% DOC/SWCNT dispersion and 425 μL of nanopure H_2O are then added to 4080 μL of the STOCK-1 solution, shortly mixed either by shaking or using a vortex mixer, and centrifuged for 5 min at 6000*g* in a fixed angle centrifuge (Thermo-Electron, model 1EC MultiRF), to induce the phase separation. After mixing the two polymers, microscopic phase-separation occurs immediately, but to separate these phases macroscopically, benchtop centrifugation is suggested. In principle, PEG and dextran alone should separate into two phases without centrifugation; however, in the presence of surfactants and salt, the macroscopic separation of the two phases may take days and therefore the centrifugation step was performed to speed up the process. Top and bottom phases were removed manually from the aggregated interface using a syringe. All separations were performed at room temperature (22 ± 2 °C). At higher temperature (30 °C), the separation yield of (6,5) SWCNTs after SP1 is decreased due to partial separation into the $SP1^T$ phase, while at lower temperature (10 °C), large diameter SWCNTs are distributed into the $SP1_B$ phase (see Figure S15), which can be attributed to the temperature-dependent surfactant dynamics on the SWCNT surface. Furthermore, small variation on surfactant concentration, *i.e.*, the use of different pipetters, can result in unwanted separation; however, as stated before the separation can be easily fixed by readjusting the surfactant concentrations.

To obtain the variations of SDS, SC and NaCl as presented in Figure 5 (and Supporting Information), different stock solutions were prepared, each time varying one component in the STOCK-1 solution. For these specific separations, the amount of SWCNTs was kept fixed, and thus intensities can directly be compared with each other. For the DOC variation in Figure 5B, the specific amount of the SWCNT dispersion and H_2O that is added to the stock solution was changed, while keeping the total volume constant to get the desired final concentration. Thus, absolute intensities cannot be compared, but relative intensities of different SWCNTs present in the suspension after sorting can.

For SP2, STOCK-2 is prepared containing: (i) 2.33 g of dextran, (ii) 14.5 g of PEG, (iii) 0.0473 g of DOC, (iv)1.8 g of SDS and (v) 100 g of nanopure H_2O. An equal amount of the bottom phase from SP1 and STOCK-2 are mixed and centrifuged as in SP1. Analogously, each parameter in STOCK-2 was changed (same as above), to obtain the spectra presented in Figure 6.

For the (7,5) separation, in SP1 we used a different SDS concentration in the STOCK-1 (0.89 g, all other parameters the same concentration) and we added 330 μL of the SWCNT dispersion and 310 μL of H_2O to make a total of 4720 μL. In SP2, the stock solution had lower SDS concentration (0.46 g). All other concentrations and separation procedures remained the same.

Dialysis of the separated SWCNT phases was performed using a pressurized filtration/stirring cell equipped with regenerated cellulose, 100 kDa membranes (Stirred Ultrafiltration Cell, Millipore). Each phase was filtered until 10% of the volume remained and then 1% (m/v) DOC solution was added to dilute the remnants by a factor of 10 leading to a minimum dilution of 10^5 for PEG, dextran and other ingredients after five cycles of filtration and dilution.

Absorption spectra were recorded with a UV−vis-NIR spectrophotometer (Cary 6000i) in the range of 200−1700 nm, using quartz cells with an optical path length of 3 mm or 1 cm.

PLE maps were acquired in a Horiba spectrometer consisting of a Gemini 180 excitation spectrometer, an iHR320 emission spectrometer and a liquid nitrogen cooled InGaAs detector. Spectra were corrected for lamp excitation, detector sensitivity, filter transmission and wavelength accuracy of the detection system.

Resonant Raman spectra were excited at multiple laser wavelengths originating either from an Ar^+-ion laser or from tunable Rhodamine 6G dye laser, Kiton-red dye laser or a Ti:sapphire laser. Spectra were recorded in backscattering geometry using a 5-5-5 Princeton Instruments TriVista triple Raman spectrometer.

Conflict of Interest: The authors declare no competing financial interest.

Acknowledgment. We acknowledge Jeffrey Fagan and Ming Zheng (NIST) for helpful discussion. This work was supported in part by the LANL LDRD program and was performed in part at the Center for Integrated Nanotechnologies, a U.S. Department of Energy, Office of Basic Energy Sciences user facility. S.C. gratefully acknowledges the financial support from the fund for scientific research Flanders, Belgium (FWO-Vlaanderen) for providing a postdoctoral fellowship and a mobility grant for visiting the Los Alamos National Laboratory. E.H.H. and A.N.G.P.-V. gratefully acknowledge support from the LANL Director's Postdoctoral Fellowship.

Supporting Information Available: Additional RRS spectra, analysis of the RRS and PLE maps, a table with the surfactant variations for SP1, additional absorption spectra of the various tests for SP1, dialysis and versatility of the separation process. This material is available free of charge *via* the Internet at http://pubs.acs.org.

REFERENCES AND NOTES

1. Jorio, A.; Dresselhaus, G.; Dresselhaus, M. S. *Carbon Nanotubes: Advanced Topics in Synthesis, Structure, Properties and Applications*; Springer-Verlag: Berlin, 2008.
2. Tu, X.; Manohar, S.; Jagota, A.; Zheng, M. DNA Sequence Motifs for Structure-Specific Recognition and Separation of Carbon Nanotubes. *Nature* **2009**, *460*, 250–253.
3. Gerstel, P.; Klumpp, S.; Hennrich, F.; Altintas, O.; Eaton, T. R.; Mayor, M.; Barner-Kowollik, C.; Kappes, M. M. Selective Dispersion of Single-Walled Carbon Nanotubes via Easily Accessible Conjugated Click Polymers. *Polym. Chem.* **2012**, *3*, 1966–1970.
4. Liu, H.; Nishide, D.; Tanaka, T.; Kataura, H. Large-Scale Single-Chirality Separation of Single-Wall Carbon Nanotubes by Simple Gel Chromatography. *Nat. Commun.* **2011**, *2*, 309.
5. Arnold, M. S.; Green, A. A.; Hulvat, J. F.; Stupp, S. I.; Hersam, M. C. Sorting Carbon Nanotubes by Electronic Structure Using Density Differentiation. *Nat. Nanotechnol.* **2006**, *1*, 60–65.
6. Khripin, C. Y.; Fagan, J. A.; Zheng, M. Spontaneous Partition of Carbon Nanotubes in Polymer-Modified Aqueous Phases. *J. Am. Chem. Soc.* **2013**, *135*, 6822–6825.
7. Albertsson, P.-A. *Partition of Cell Particles and Macromoleucles*, 2nd ed.; Wiley- Interscience: Hoboken, NJ, 1971.
8. Fagan, J. A.; Khripin, C. Y.; Silvera Batista, C. A.; Simpson, J. R.; Hároz, E. H.; Hight Walker, A. R.; Zheng, M. Isolation of Specfic Small Diameter Single-Wall Carbon Nanotube Species *via* Aqueous Two-Phase Extraction. *Adv. Mater.* **2014**, 10.1002/adma.201304873.
9. Zhao, P.; Einarsson, E.; Lagoudas, G.; Shiomi, J.; Chiashi, S.; Maruyama, S. Tunable Separation of Single-Walled Carbon Nanotubes by Dual-Surfactant Density Gradient Ultracentrifugation. *Nano Res.* **2011**, *4*, 623–634.
10. Shastry, T. A.; Morris-Cohen, A. J.; Weiss, E. A.; Hersam, M. C. Probing Carbon Nanotube–Surfactant Interactions with Two-Dimensional DOSY NMR. *J. Am. Chem. Soc.* **2013**, *135*, 6750–6753.
11. Niyogi, S.; Boukhalfa, S.; Chikkannanavar, S. B.; McDonald, T. J.; Heben, M. J.; Doorn, S. K. Selective Aggregation of Single-Walled Carbon Nanotubes *via* Salt Addition. *J. Am. Chem. Soc.* **2007**, *129*, 1898–1899.
12. Niyogi, S.; Densmore, C. G.; Doorn, S. K. Electrolyte Tuning of Surfactant Interfacial Behavior for Enhanced Density-Based Separations of Single-Walled Carbon Nanotubes. *J. Am. Chem. Soc.* **2009**, *131*, 1144–1153.
13. Matsuoka, K.; Moroi, Y. Micelle Formation of Sodium Deoxycholate and Sodium Ursodeoxycholate (Part 1). *Biochim. Biophys. Acta, Mol. Cell Biol. Lipids* **2002**, *1580*, 189–199.
14. Tsyboulski, D. A.; Rocha, J.-D. R.; Bachilo, S. M.; Cognet, L.; Weisman, R. B. Structure-Dependent Fluorescence Efficiencies of Individual Single-Walled Carbon Nanotubes. *Nano Lett.* **2007**, *7*, 3080–3085.
15. Bonaccorso, F.; Hasan, T.; Tan, P. H.; Sciascia, C.; Privitera, G.; Di Marco, G.; Gucciardi, P. G.; Ferrari, A. C. Density Gradient Ultracentrifugation of Nanotubes: Interplay of Bundling and Surfactants Encapsulation. *J. Phys. Chem. C* **2010**, *114*, 17267–17285.
16. Cambre, S.; Wenseleers, W. Separation and Diameter-Sorting of Empty (End-Capped) and Water-Filled (Open) Carbon Nanotubes by Density Gradient Ultracentrifugation. *Angew. Chem., Int. Ed.* **2011**, *50*, 2764–2768.
17. Fagan, J. A.; Zheng, M.; Rastogi, V.; Simpson, J. R.; Khripin, C. Y.; Batista, C. A. S.; Walker, A. R. H. Analyzing Surfactant Structures on Length and Chirality Resolved (6,5) Single-Wall Carbon Nanotubes by Analytical Ultracentrifugation. *ACS Nano* **2013**, *7*, 3373–3387.
18. Poulin, P.; Vigolo, B.; Launois, P. Films and Fibers of Oriented Single Wall Nanotubes. *Carbon* **2002**, *40*, 1741–1749.
19. Wenseleers, W.; Vlasov, I. I.; Goovaerts, E.; Obraztsova, E. D.; Lobach, A. S.; Bouwen, A. Efficient Isolation and Solubilization of Pristine Single-Walled Nanotubes in Bile Salt Micelles. *Adv. Funct. Mater.* **2004**, *14*, 1105–1112.
20. Lin, S.; Blankschtein, D. Role of the Bile Salt Surfactant Sodium Cholate in Enhancing the Aqueous Dispersion Stability of Single-Walled Carbon Nanotubes: A Molecular Dynamics Simulation Study. *J. Phys. Chem. B* **2010**, *114*, 15616–15625.
21. Tummala, N. R.; Striolo, A. SDS Surfactants on Carbon Nanotubes: Aggregate Morphology. *ACS Nano* **2009**, *3*, 595–602.
22. Duque, J. G.; Densmore, C. G.; Doorn, S. K. Saturation of Surfactant Structure at the Single-Walled Carbon Nanotube Surface. *J. Am. Chem. Soc.* **2010**, *132*, 16165–16175.
23. O'Connell, M. J.; Sivaram, S.; Doorn, S. K. Near-Infrared Resonance Raman Excitation Profile Studies of Single-Walled Carbon Nanotube Intertube Interactions: A Direct Comparison of Bundled and Individually Dispersed HiPco Nanotubes. *Phys. Rev. B* **2004**, *69*, 235415.
24. Duque, J. G.; Parra-Vasquez, A. N. G.; Behabtu, N.; Green, M. J.; Higginbotham, A. L.; Price, B. K.; Leonard, A. D.; Schmidt, H. K.; Lounis, B.; Tour, J. M.; *et al.* Diameter-Dependent Solubility of Single-Walled Carbon Nanotubes. *ACS Nano* **2010**, *4*, 3063–3072.
25. Duque, J. G.; Oudjedi, L.; Crochet, J. J.; Tretiak, S.; Lounis, B.; Doorn, S. K.; Cognet, L. Mechanism of Electrolyte-Induced Brightening in Single-Walled Carbon Nanotubes. *J. Am. Chem. Soc.* **2013**, *135*, 3379–3382.
26. Duque, J. G.; Pasquali, M.; Cognet, L.; Lounis, B. Environmental and Synthesis-Dependent Luminescence Properties of Individual Single-Walled Carbon Nanotubes. *ACS Nano* **2009**, *3*, 2153–2156.
27. Green, A. A.; Hersam, M. C. Colored Semitransparent Conductive Coatings Consisting of Monodisperse Metallic Single-Walled Carbon Nanotubes. *Nano Lett.* **2008**, *8*, 1417–1422.